



UNIVERSITY OF LEEDS

This is a repository copy of *Data-Driven Dynamic Modeling of Coupled Thermal and Electric Outputs of Microturbines*.

White Rose Research Online URL for this paper:
<http://eprints.whiterose.ac.uk/132434/>

Version: Accepted Version

Article:

Xu, X, Li, K orcid.org/0000-0001-6657-0522, Jia, H et al. (3 more authors) (2018)
Data-Driven Dynamic Modeling of Coupled Thermal and Electric Outputs of Microturbines.
IEEE Transactions on Smart Grid, 9 (2). pp. 1387-1396. ISSN 1949-3053

<https://doi.org/10.1109/TSG.2016.2590022>

© 2016 IEEE. This is an author produced version of a paper published in IEEE Transactions on Smart Grid. Personal use of this material is permitted. Permission from IEEE must be obtained for all other uses, in any current or future media, including reprinting/republishing this material for advertising or promotional purposes, creating new collective works, for resale or redistribution to servers or lists, or reuse of any copyrighted component of this work in other works. Uploaded in accordance with the publisher's self-archiving policy.

Reuse

Items deposited in White Rose Research Online are protected by copyright, with all rights reserved unless indicated otherwise. They may be downloaded and/or printed for private study, or other acts as permitted by national copyright laws. The publisher or other rights holders may allow further reproduction and re-use of the full text version. This is indicated by the licence information on the White Rose Research Online record for the item.

Takedown

If you consider content in White Rose Research Online to be in breach of UK law, please notify us by emailing eprints@whiterose.ac.uk including the URL of the record and the reason for the withdrawal request.



eprints@whiterose.ac.uk
<https://eprints.whiterose.ac.uk/>

Data-Driven Dynamic Modeling of Coupled Thermal and Electric Outputs of Microturbines

Xiandong Xu, *Member, IEEE*, Kang Li, *Senior Member, IEEE* Hongjie Jia, *Member, IEEE*, Xiaodan Yu, Jing Deng, and Yunfei Mu *Member, IEEE*,

Abstract—Microturbines are among the most successfully commercialized distributed energy resources, especially when they are used for combined heat and power generation. However, the interrelated thermal and electrical system dynamic behaviors have not been fully investigated. This is technically challenging due to the complex thermo-fluid-mechanical energy conversion processes, which introduce multiple time-scale dynamics and strong nonlinearity into the analysis. To tackle this problem, this paper proposes a simplified model which can predict the coupled thermal and electric output dynamics of microturbines. Considering the time-scale difference of various dynamic processes occurring within microturbines, the electromechanical subsystem is treated as a fast quasi-linear process, while the thermo-mechanical subsystem is treated as a slow process with high nonlinearity. A three-stage subspace identification method is utilized to capture the dominant dynamics and predict the electric power output. For the thermo-mechanical process, a radial basis function model trained by the particle swarm optimization method is employed to handle the strong nonlinear characteristics. Experimental tests on a Capstone C30 microturbine show that the proposed modeling method can well capture the system dynamics, and produce a good prediction of the coupled thermal and electric outputs in various operating modes.

Index Terms—Microturbine, combined heat and power, dynamic behavior, modeling, system identification.

NOMENCLATURE

Abbreviations

| | |
|--------|---|
| CHP | Combined heat and power. |
| MT | Microturbine. |
| DN | Distribution network. |
| DERs | Distributed energy resources. |
| NARMAX | Nonlinear autoregressive moving average with exogenous inputs models. |
| NARX | Nonlinear autoregressive exogenous. |
| PSO | Particle swarm optimization. |
| RBF | Radial basis function. |
| N4SID | Subspace state space system identification. |
| PDEs | Partial differential equations. |
| AIC | Akaike information criterion. |

This work was supported by the Engineering and Physical Sciences Research Council (EPSRC) under Grant No. EP/L001063/1 and EP/P004636/1, the Distinguished Visiting Fellowship Scheme of the Royal Academy of Engineering (DVF1415/2/59), the National Science Foundation of China (No. 51377117), and the National High-tech R&D Program of China (No. 2015AA050403).

X. Xu, K. Li, and J. Deng are with the School of Electronics, Electrical Engineering and Computer Science, Queens University Belfast, Belfast BT9 5AH, UK (e-mail: x.xu@qub.ac.uk; k.li@qub.ac.uk; j.deng@qub.ac.uk).

H. Jia, X. Yu, and Y. Mu are with the Key Laboratory of Smart Grid of Ministry of Education, Tianjin University, Tianjin, 300072, China (e-mail: hjia@tju.edu.cn; yuxd@tju.edu.cn; yunfeimu@tju.edu.cn).

| | |
|------|---------------------------------|
| MSE | Mean squared error. |
| MAPE | Mean absolute percentage error. |

Notation

| | |
|----------------------|--|
| x_t, y_t | State and algebraic variables of the thermo-mechanical system. |
| x_e, y_e | State and algebraic variables of the electro-mechanical system. |
| f_t | Thermo-mechanical system model. |
| f_e | Electro-mechanical system model. |
| g | Algebraic links between f_t and f_e . |
| p | Position variables. |
| f_{es}, f_{ef} | Slow and fast subsystems of the electro-mechanical system. |
| x_{es}, x_{ef} | Slow and fast variables of x_s . |
| $\hat{x}_{es}(k)$ | State vector at time k |
| $u(k), \hat{y}_e(k)$ | Input and output vectors at time k . |
| $\omega(k), v(k)$ | Vectors of Gaussian distributed, zero mean, white noise sequences. |
| A, B, C, D | System model matrices. |
| \hat{y}_t | RBF network output. |
| y | Actual output. |
| x | Input vector. |
| λ_i | Output layer weight of the i th hidden node. |
| σ_i, c_i | Center and width vectors of Gaussian function of the i th hidden node. |
| J | Estimated residual of the fitted model. |
| d | Total number of estimated parameters. |
| N_e, N_t | Data record length of the electro-mechanical and thermo-mechanical subsystems. |
| ω^{upper} | Upper bound of the MT rotational speed. |
| P_{out} | Electro-mechanical model output. |

I. INTRODUCTION

A new trend in the smart grid related studies is to integrate multiple energy systems, especially at the microgrid level [1]. As one of the most successful commercial applications of microgrids, combined heat and power (CHP) has drawn a lot of interest in recent years due to its high efficiency and low emission characteristics [2]. As the key component of the CHP, microturbines (MT) can generate heat and electricity simultaneously and thus have a significant impact on the operation of both local energy services and the distribution network (DN) [3]. In addition, MTs are widely used to smooth other distributed energy resources (DERs) output fluctuations and meet other requirements of the DN, due to their advantage

of higher reliability, faster response, and so on. In order to better manage the MT and CHP at both the microgrid and the DN levels, an essential step is to develop an appropriate model that can capture the relationship between the manipulated input variables and the power and heat outputs.

However, in practice, MTs exhibit complex thermo-fluid-mechanical energy conversion processes with strong nonlinearity [4]. Heat and power outputs of MTs depend on both control actions and internal characteristics. For example, if a MT is operated in parallel with the utility, and set to follow the heat load, thermal system variation will affect the power output and the DN operation simultaneously. Moreover, different time scales and complex coupling of thermal and electric processes make it more difficult to consider the two subsystem dynamics in a unified model. To capture interrelations between the two subsystems, establishing comprehensive yet simple enough models becomes a crucial but challenging part of MT studies.

In the literature, MT modeling methods can be grouped into two categories. One commonly used method is based on mechanism analysis of various subsystems, including thermo-mechanical subsystems [5], electric converters [6], the correlation between the electric and thermo-mechanical subsystems [7], the fuel control system [8], etc. The main limitations of these methods include: 1) the models are often developed near the rated operating points; 2) some internal parameters are confidential, and thus hardly accessible; 3) operating saturations caused by low pressure gas networks are not well considered.

Data-driven identification offers an alternative approach to model systems with strong nonlinearity and unknown parameters. It has been employed in various engineering applications, such as power plant emission prediction [9], communication systems [10], polymer extrusion processes [11], etc. For modeling MTs, different types of black-box models, such as nonlinear autoregressive moving average with exogenous inputs models (NARMAX) [12], nonlinear autoregressive exogenous (NARX) [13], neural network models [14], [15], and adaptive network-based fuzzy inference systems [16], have been used to capture gas turbine dynamics. Those models have been proved effective in capturing the relationship between fuel consumption and mechanical power output for a specific MT. However, MTs may be owned by different third-parties, thus the required operational data may not be fully available for utilities. System operators may not be able to build identification models from available data for assessing the dynamic impacts of MTs on utilities and customers. Therefore, a priori knowledge is needed to incorporate the interactions between thermo-mechanical and electro-mechanical subsystems within the CHP.

In this paper, a data-driven MT modeling method is proposed combined with singular perturbation theories. The main contributions are summarized as follows: 1) the feasibility of building a simplified MT model is analyzed based on its time-scale characteristics; 2) the electro-mechanical subsystem is modeled by a three-stage subspace identification method to predict the MT power output under different operating conditions; 3) the thermo-mechanical subsystem is modeled by a particle swarm optimization (PSO) assisted radial basis

function (RBF) by correlating the power output with the heat output. Experimental results confirm that, with the proposed method, a simplified model is able to represent the complex energy conversion process in MTs and to produce accurate predictions of the coupled power and heat outputs.

II. MECHANISM OF MT OPERATION

A microgrid with multiple energy systems is presented in Fig. 1(a). It consists of a MT, a solar panel, energy storage systems, an air-conditioner, and various types of loads. As highlighted in the dotted green cycle, electric, gas, and heat systems become interrelated due to the existence of the MT. From the view point of the utility, the microgrid can be operated in two modes. In the islanded mode, without the support of the electrical grid, heat and power energy balances are closely related to MT outputs. In the grid-tied mode, the microgrid can exchange power with an external network, which indicates that the MT output adjustment (both heat and power) can affect the DN operation. The natural gas network, as the energy source of the MT, can also affect the microgrid operation. Therefore, it is necessary to model the MT in order to identify interactions among various systems and to assist the microgrid management.

A. MT Model

In practice, MTs present diverse structures. This paper focuses on a single-shaft MT that is widely used to meet local energy demands. As illustrated in Fig. 1(b), the MT consists

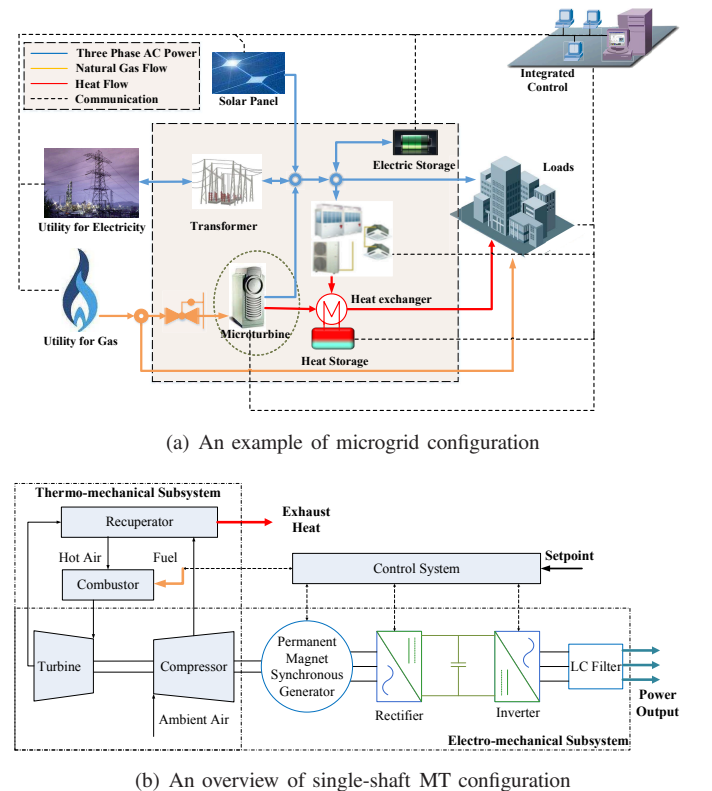


Fig. 1. Configurations of a microgrid and the embedded MT

of a gas turbine, a permanent magnet synchronous generator, and electronic converters. The general form of the model can be expressed as

$$\begin{cases} \dot{x}_t = f_t\left(\frac{\partial x_t}{\partial p}, x_t, y_t, u, x_e, y_e\right) \\ \dot{x}_e = f_e(x_t, y_t, u, x_e, y_e) \\ 0 = g(x_t, y_t, u, x_e, y_e) \end{cases} \quad (1)$$

where f_t and f_e represent thermo-mechanical and electro-mechanical subsystem models, respectively, and g links these two models algebraically. x_t represents thermo-mechanical subsystem state variables, such as the engine speed, the fuel flow pressure, the component temperature, etc. p represents position variables. y_t stands for thermo-mechanical subsystem algebraic variables which includes the exhaust gas temperature, the flow, etc. x_e represents electro-mechanical subsystem state variables, including the generator angle, converter control system states, etc. y_e represents electro-mechanical subsystem algebraic variables, including the generator power output, and the voltage, etc. u represents the control signal of the MT.

The electro-mechanical subsystem of the MT is closely related to the DN analysis. Due to significant differences in their response characteristics, thermo-mechanical subsystem variables x_t can be considered constant when analyzing the electro-mechanical process. It has also been found that some state variables dominate the MT dynamics [17]. Based on the singular perturbation theory, the MT can be further described as a cascaded system below:

$$\begin{cases} \dot{x}_{es} = f_{es}(x_t, y_t, u, x_e, y_e) \\ \epsilon \dot{x}_{ef} = f_{ef}(x_t, y_t, u, x_e, y_e) \\ 0 = g(x_t, y_t, u, x_e, y_e) \end{cases} \quad (2)$$

where ϵ is a small non-negative scalar. x_{es} and x_{ef} represent slow and fast variables of x_e . f_{es} and f_{ef} represent slow and fast subsystems of the electro-mechanical system.

By setting $\epsilon = 0$, the fast dynamics of x_e can be further described by the algebraic equation f_{ef} for long-term studies. Inspired by the two-time-scale theory in the hybrid energy system [8] and electric power systems [18], the dominant model (considered as the slow subsystem here) of the MT's electro-mechanical subsystem can be modeled as follows:

$$\begin{cases} \dot{x}_{es} = f_{es}(x_t, y_t, u, x_e, y_e) \\ 0 = f_{ef}(x_t, y_t, u, x_e, y_e) \\ 0 = g(x_t, y_t, u, x_e, y_e) \end{cases} \quad (3)$$

B. Heat and Output Control

To maximize the energy efficiency, the MT is usually used to produce combined heat and power. According to the objectives, two types of control methods are often used in the MT management, namely heat tracking and electricity tracking [19], as illustrated in Fig. 2.

In the electricity tracking mode, the control system is designed to follow various electrical system requirements. For example, if the MT is used as a slack bus in the DN operation, the reference signal will be set to the rated frequency. Furthermore, the MT can be set to follow electric load variations. In

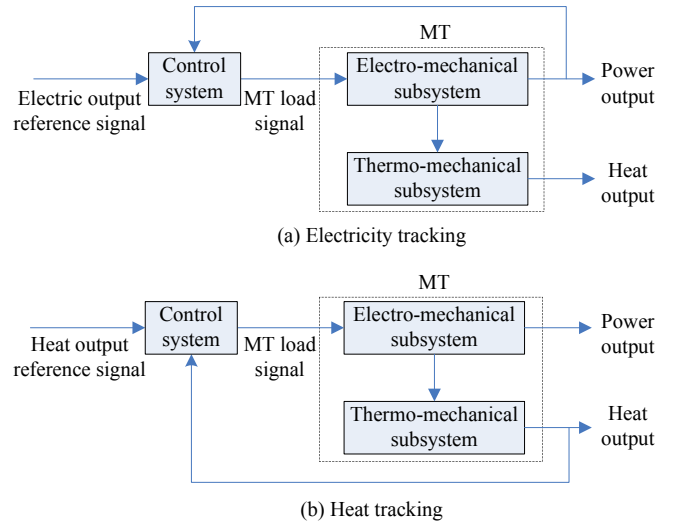


Fig. 2. MT electricity and heat output control

both scenarios, the electricity control signals are converted to the MT load signals and transmitted to the MT. To handle the heat load mismatch, the dynamics of the thermo-mechanical subsystem needs to be modeled.

In the heat tracking mode, the MT output is set to follow the heat demand. The surplus/deficit electricity is balanced by the utility, which implies that the heat load could affect the DN directly in addition to the electric load variation. Compared with the electric system, the response of the thermal system to control signals is much slower, and therefore requires a long-term dynamic model of MTs.

Considering different operating mechanisms and response characteristics, the heat and power output could be described by cascaded models in the two operating modes. In the following, the MT will be modeled in a unified framework.

III. INTEGRATED MODELING METHOD

In this paper, an integrated modeling method is proposed as shown in Fig. 3. The MT can be described by a cascaded model as aforementioned. Thermo-mechanical and electro-mechanical subsystems are considered as two single-input single-output systems. The power output is considered as the interconnection between the two subsystems. The electro-mechanical subsystem is modeled by using a subspace identification method in order to represent key dynamics of the model, while the thermo-mechanical subsystem is described by the RBF model which has broad approximation capabilities. The detailed procedure to build the MT model is presented below.

Input and output data collection. Load signals are acquired from control systems in the two operating modes. Different control objectives of the MT should be identified in order to obtain input and output signals. The power and heat outputs are collected as outputs of the MT. According to various customer requirements, electric load signals and power outputs, which play a key role in the DN operation, are selected as inputs and outputs of the electro-mechanical subsystem. The power

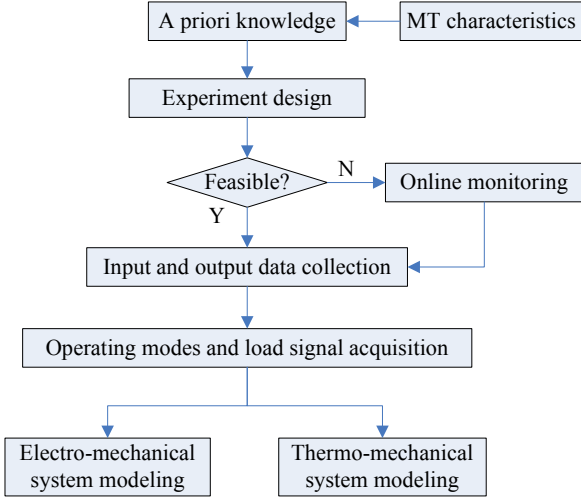


Fig. 3. Framework of the integrated modeling method

output, which incorporates both load and disturbance signals of the system, is selected as the input of the thermo-mechanical subsystem model instead of the load signal.

Electro-mechanical subsystem modeling: To ensure the operating efficiency, MTs are usually operated within a certain range¹ of the engine speed in normal operating conditions. It has been shown that the electro-mechanical subsystem of MTs exhibits a good linearity in the operating range [17]. This allows the MT model (3) to be built in the studied range using the linear state space model (4), which can estimate both system outputs and state variables. Considering the existence of measurement noise in the field data, the subspace state space system identification (N4SID) [20] is employed to identify unknown parameters in (4).

$$\begin{cases} \hat{\mathbf{x}}_{es}(k+1) = \mathbf{A}\hat{\mathbf{x}}_{es}(k) + \mathbf{B}\mathbf{u}(k) + \boldsymbol{\omega}(k) \\ \hat{\mathbf{y}}_e(k) = \mathbf{C}\hat{\mathbf{x}}_{es}(k) + \mathbf{D}\mathbf{u}(k) + \mathbf{v}(k) \end{cases} \quad (4)$$

where \mathbf{A} , \mathbf{B} , \mathbf{C} , and \mathbf{D} represent the system model matrixes, $\hat{\mathbf{x}}_{es}(k)$, $\mathbf{u}(k)$ and $\hat{\mathbf{y}}_e(k)$ represent state, input and output vector at time k , $\boldsymbol{\omega}(k)$ and $\mathbf{v}(k)$ are vectors of Gaussian distributed, zero mean, white noise sequences, $k = 1, 2, \dots, N_e$, N_e is the length of the electro-mechanical system data record.

Thermo-mechanical subsystem modeling: The thermo-mechanical subsystem includes the combustion process, the heat transfer process, the heat exchanger, etc. The whole process is described by partial differential equations (PDEs) with strong nonlinearity. It has been shown that the solution could be represented by superposition and composition of continuous functions of single variables [21]. In the section below, we will use the RBF neural model to describe such underlying functions due to their simple topological structure and universal approximation ability. A general representation of the RBF network with m hidden nodes can be written as [22]

$$\hat{y}_t(j) = \sum_{i=1}^m \lambda_i \phi_i(\mathbf{x}(j), \sigma_i, c_i) = \boldsymbol{\Phi} \boldsymbol{\Lambda} \quad (5)$$

¹The range can be obtained by monitoring the operational data of MTs.

where $\hat{\mathbf{y}}_t = [\hat{y}_t(1), \hat{y}_t(2), \dots, \hat{y}_t(N_t)]^T$ represents the RBF network output vector, N_t is the number of thermo-mechanical subsystem data samples, $\mathbf{x}(j)$ represents the input vector to the network including input and output variables at time j , λ_i represents the linear output weight of the i th hidden node, $\boldsymbol{\Lambda} = [\lambda_1, \lambda_2, \dots, \lambda_m]^T$. $\phi_i(\mathbf{x}(j), \sigma_i, c_i)$ represents the RBF of the i th hidden node at time j , $\boldsymbol{\Phi} = [\phi_1, \phi_2, \dots, \phi_m]$. In this paper, the Gaussian function is employed as the basis function because of its good approximation capability, $\mathbf{c} = [c_1, c_2, \dots, c_m]^T$ and $\boldsymbol{\sigma} = [\sigma_1, \sigma_2, \dots, \sigma_m]^T$ represent the center and width vectors of the Gaussian function.

Let $\mathbf{y}_t = [y_t(1), y_t(2), \dots, y_t(N_t)]^T$ be the actual output vector, then the network training aims to optimize \mathbf{c} , $\boldsymbol{\sigma}$, and $\boldsymbol{\Lambda}$ to minimize the sum squared error

$$Q(\boldsymbol{\sigma}, \mathbf{c}, \boldsymbol{\Lambda}) = \sum_{j=1}^{N_t} [y_t(j) - \hat{y}_t(j)]^2 \rightarrow \min \quad (6)$$

The corresponding least square estimation of the linear output weight $\boldsymbol{\Lambda}$ can be given by $\hat{\boldsymbol{\Lambda}} = (\boldsymbol{\Phi}^T \boldsymbol{\Phi})^{-1} \boldsymbol{\Phi}^T \mathbf{y}$ [22].

From a practical viewpoint, both the N4SID and RBF models have computational problems which need to be solved.

- In the N4SID model, the system order must be properly selected to comprise the computational burden and the model accuracy. Moreover, nonlinear characteristics should be incorporated in order to deal with the internal state and output saturations in the electro-mechanical subsystem. To handle these issues, a three-stage modeling method will be presented in order to describe the electro-mechanical subsystem dynamic behaviors.
- In the RBF model, the widths and centers of the Gaussian functions need to be selected in order to guarantee good approximation performance. Also, considering the correlations and noise between regressors, the information matrix $\boldsymbol{\Phi}^T \boldsymbol{\Phi}$ is usually ill-conditioned, which may affect the accuracy of the model coefficient calculation. Therefore, it is crucial to select the most relevant and significant terms from the candidate model set, to ensure the accuracy, as well as the computational cost of the surrogate model. To achieve this goal, a PSO-assisted RBF network will be applied in the thermo-mechanical subsystem modeling, for predicting the heat output related to the power output.

IV. COMPUTATIONAL PROCEDURE

The computational procedure for implementing the integrated modeling approach is presented below. The flowchart of the electro-mechanical subsystem modeling is shown in Fig. 4, and the flowchart of the thermo-mechanical subsystem modeling is described in Fig. 5. Details regarding the implementation of the approach are given in the following subsections.

A. Electro-mechanical Subsystem Modeling

As illustrated in Fig. 4, a three-stage subspace identification method is proposed to model the electro-mechanical subsystem. A priori knowledge of MT dynamics is utilized to determine the system order, and to incorporate system

state saturation nonlinearity. The detailed modeling process is presented below.

Stage I: System Order Estimation.

Step 1: Estimate the system order based on mechanism analysis and historic information.

Step 2: Acquire data by monitoring the system operation and/or specifically designed physical experiments.

Stage II: System Identification.

Step 3: Collect a sequence of input $U_0, U_1, \dots, U_{2i-1}$ and output $Y_0, Y_1, \dots, Y_{2i-1}$ data vectors defined in the previous section (load signals and actual electric power outputs).

Step 4: Check if the system order n_x is specified in the preprocessed data. If specified, the N4SID is utilized to identify the system with n_x as the number of relatively large singular values (for details, see Appendix A). If not, based on the information theory, a heuristic way will be utilized to seek the model that has a good fit to the actual data, but has few parameters. In this paper, the Akaike Information Criterion (AIC), which takes into account the number of parameters and the sample size, is employed to select an appropriate order for the state space model [20]. The AIC can be calculated by

$$AIC = \ln\left(J\left(1 + 2\frac{d}{N_e}\right)\right) \quad (7)$$

where d is the total number of estimated parameters, J is

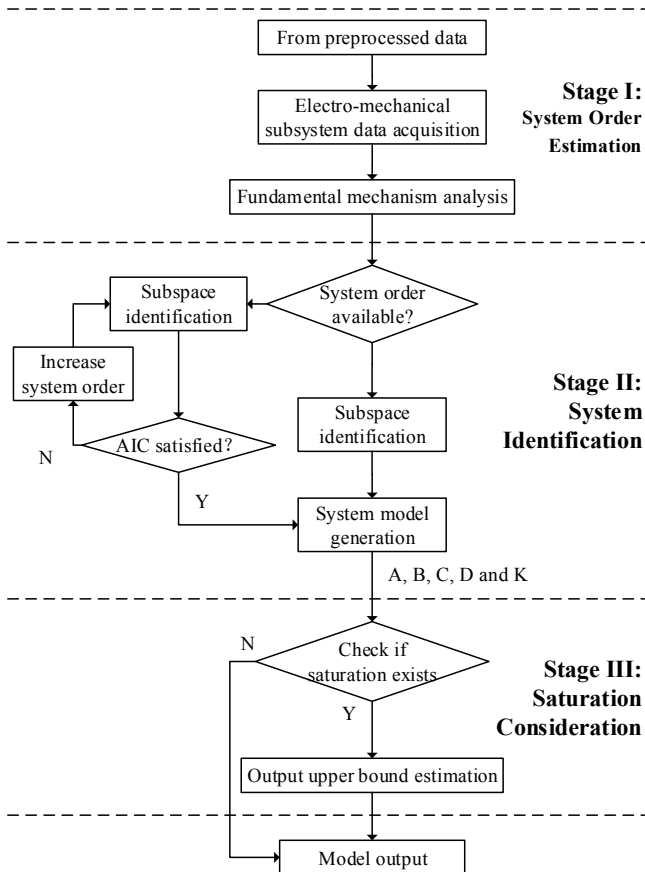


Fig. 4. Flowchart of the electro-mechanical system identification process.

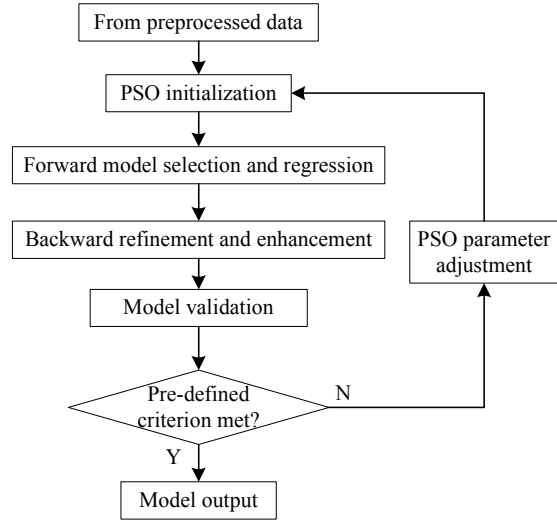


Fig. 5. Flowchart of the thermo-mechanical subsystem modeling process.

the estimated residual of the fitted model, calculated by $J = \sum_{t=1}^{N_e} [y_e(t) - \hat{y}_e(t)]^2$.

Step 5: Calculate A, B, C, D as a system model estimation.

Stage III: Saturation Consideration.

Step 6: Check if a saturation exists in the obtained data. In the MT, the gas pressure is regulated by adjusting compressor and valve positions to maintain the fuel intake at a certain level. At a low fuel pressure level, the MT power output will be constrained when the engine speed reaches its upper bound. To capture the MT output constraints, the saturation region of the engine speed is monitored to adjust the model developed in Stage II.

Step 7: By comparing the estimated states with the normalized observed states, the engine speed upper bound ω^{upper} can be estimated. To ensure system operation security, a conservative upper bound is often used. Then the model output P_{out} can be estimated as follow:

$$P_{out} = \begin{cases} \hat{y}_e(k), \hat{x}_{es}(k+1) \leq \omega^{upper} \\ P_{out}^{upper}, \hat{x}_{es}(k+1) > \omega^{upper} \end{cases} \quad (8)$$

Step 8: Model output: Design another group of sample data to test the performance of the obtained model. If the error is within the limit, then output the results.

B. Thermo-mechanical Subsystem Modeling

To deal with the issues of the RBF model mentioned in the previous section, the PSO is employed to determine the width and the center in each RBF node selection process [23]. The fast recursive algorithm in [24] is utilized to select a small set of RBF nodes and handle the ill-condition in a traditional least square estimation method. Then the RBF network structure is adjusted according to the net contribution of each hidden node. The flowchart of the method is presented in Fig. 5. A brief introduction of the modeling method is presented as follows.

Step 1: Input and output selection: Acquire and preprocess experimental data. The electric output P_{out} , which is coupled

with the heat output, can reflect the impact of disturbances on the MT output. Therefore, P_{out} is selected as the RBF model input. Exhaust gas temperature T_{ex} which can be easily monitored is chosen as the RBF model output to reflect the slow dynamics of the MT heat output.

Step 2: PSO and RBF model initialization: Initialize the PSO items, including the size of the swarm, the maximum number of PSO iterations, the position range of the particles, the velocity range of the particles, and the weight for the velocity updating. Assign the particle solution to σ and c and construct the corresponding candidate RBF basis vector as the initial model for the next step.

Step 3: Forward model selection and regression: With the initialized model, a residual matrix from the fast recursive algorithm is adopted in the RBF. Hereby, the mean square error (MSE) is employed as an estimator of the deviations between the model output and the actual data. By integrating with the PSO, σ and c are iteratively trained to minimize the MSE. The selection process terminates until a criterion is satisfied such as the AIC or a maximum number of centers have been added. The MSE of the model (5) is defined as

$$MSE = \frac{1}{N_t} \sum_{j=1}^{N_t} (y_t(j) - \hat{y}_t(j))^2 \quad (9)$$

Step 4: Backward network performance enhancement: In this step, various hidden nodes are moved to the last position in the full regression matrix of the RBF model. The nonlinear parameters of the hidden nodes are then adjusted by using a similar way as for the fast recursive algorithm. During the iteration process, abundant hidden nodes should be pruned while necessary nodes may be added into the network in some cases. When the performance of the obtained model is acceptable, the whole RBF neural model refinement procedure is then terminated; otherwise, start a new performance enhancement loop.

Step 5: Model parameter identification: With the obtained terms in Step 4, the output layer weight vector of the RBF can be calculated using a back substitution (see [24] for details).

Step 6: Model validation and output: If the pre-defined criterion is not satisfied, adjust the PSO parameter and then go to Step 2; otherwise, stop.

V. CASE STUDIES

In smart grid applications, the MT is usually accessed to microgrids in order to meet heat and power demands of customers. It also plays a key role in smoothing the fluctuations of renewable outputs, such as wind and solar power, and in assisting energy management and control of microgrids. Therefore, the case studies are conducted in the microgrid testbed with a Capstone C30 MT located at the Smart Grid Laboratory of Tianjin University [25]. The microgrid consists of multiple DERs, and it supplies energy to loads in forms of heat and power. As shown in Fig. 6, the MT obtains fuel from a local gas network that also supplies gas to the dining room near the lab. Similar to the negative effect of a low pressure gas network on the gas-fired power plant [26], it has been observed that the gas consumption of the dining room can

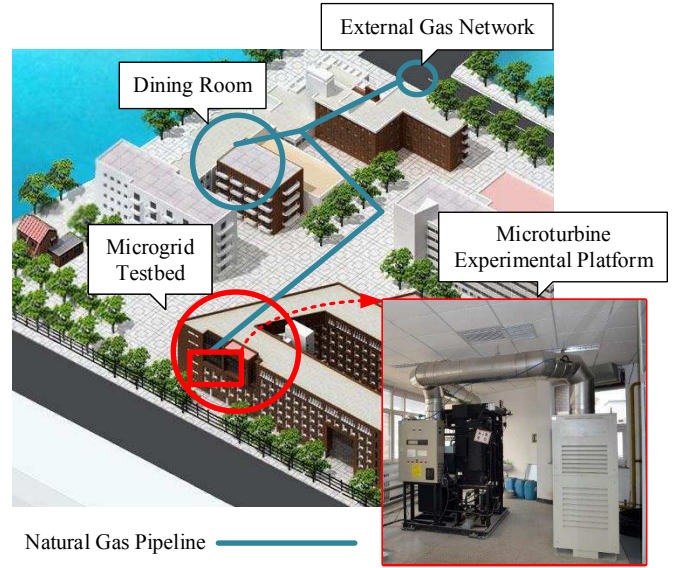


Fig. 6. MT experimental platform and the natural gas supply network of its surrounding areas.

affect the MT output in the lab, particularly during meal times when the gas load level in the whole network is high, which may cause output adjustment failures in microgrids. This effect makes the lab an ideal place for investigating the impact of the natural gas network on the smart grid operation through MTs. Incorporating this effect, the proposed modeling method is applied to modeling the MT and identifying the relationship between its heat and power outputs. The rated power of the MT is 30 kW. Detailed parameters can be found in [27]. It is accessed to a 380 V low voltage distribution network and a 5 kPa natural gas network. Measurements are recorded at a rate of 4 samples per second. The operating data is collected through remote monitoring software and the user interface port of the MT. Datasets of the load signal, the power output, and the exhaust gas temperature from physical experiments are used to assess the ability of the integrated modeling method, to characterize the coupled heat and power output behaviors of the MT.

A. Implementation of Model Identification

As mentioned earlier, the MT power output P_{out} is usually set above a certain value in order to ensure the operating efficiency. Thus, a load signal ranging above 5 kW is chosen to cover the normal operating range. The reactive power output of the MT is set to zero in the whole process. Three model order selection methods are compared to illustrate the effectiveness of the proposed method as follows.

Dominant order selection: It has been suggested that MTs behave as a 2^{nd} order system [17][28], which indicates that some state variables dominate the MT dynamics. Thus, a 2^{nd} order model is built using N4SID.

AIC based order selection: The AIC, which is a part of the modeling method, is also utilized to select the system order. As shown in Fig. 7, the minimum AIC is obtained at system

order 7 and the AIC has almost no change when the system order is larger than 7. Thus, the final model order is set to 7.

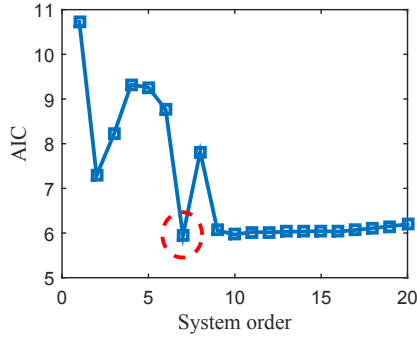


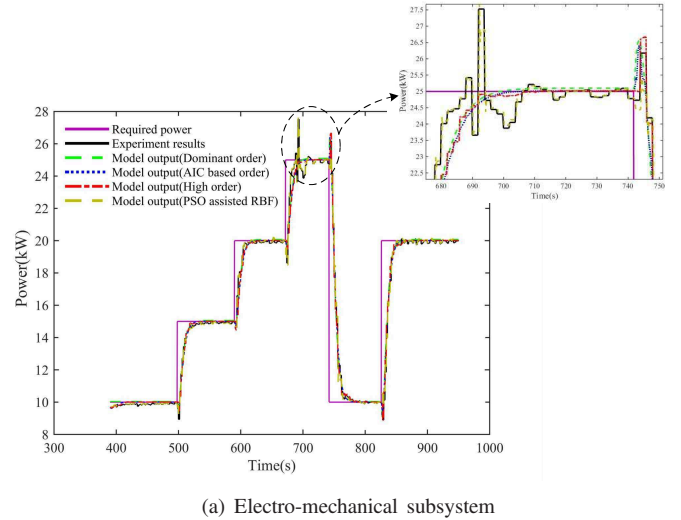
Fig. 7. The AIC of different system orders.

High order system: Due to the existence of the thermal energy conversion process, the MT model can be described by PDEs which is an infinite dimension system. Generally speaking, a high order model could approximate the PDEs process better. Thus, a high order system (80th model for example) is simulated for comparison purposes.

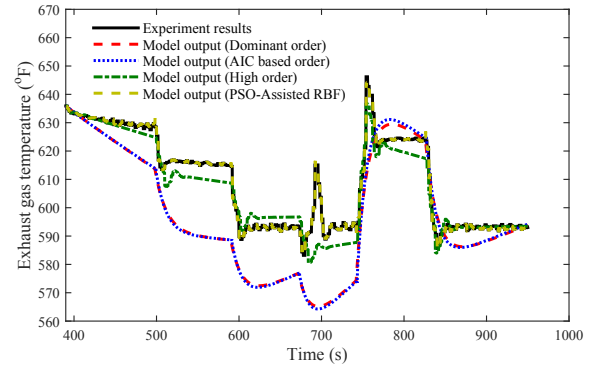
To incorporate various impact factors, such as the pressure level difference of the gas supply network, two groups of data are acquired by monitoring the MT operation over different periods of time. The first group is employed for model identification in the normal range, and the second is used for model saturation correction.

1) *Model Identification:* In the first group, the MT is operated in a normal operating range. The model is firstly obtained using the proposed three-stage method. The relative outputs of the models with different orders are shown in Fig. 8(a). As previously informed, a higher order model provides more accurate information, thus, the AIC model (dotted blue line) potentially can provide better results than the lower order dominant model (dashed green line). Both models show certain mismatches in small scales. The high order model shows better performance for short-term prediction of fluctuation behaviors (see the dashed dotted red line). It can be found that all three models produce a good approximation of the experimental data, although minor mismatches exist. For comparison, the power output in the case of the PSO-assisted RBF network is also utilized to describe the input and output behaviors of the MT electro-mechanical subsystem. Due to the nonlinear approximation capability, the RBF network can estimate the power output better in small scales, as shown in Fig. 8(a). However, it cannot give MT internal state estimation, which is required for the electric power system dynamic analysis. Since the developed model is used for analyzing dynamic impacts of MTs on microgrids and the DN, the models obtained from the N4SID will be chosen in most scenarios.

To be consistent with electro-mechanical subsystem tests, thermo-mechanical subsystem data is collected for the same time periods with the above test. Here, exhaust gas temperature T_{ex} is used as an index to reflect the heat output. For comparison purposes, both the proposed PSO assisted RBF network and the N4SID method are adopted to model T_{ex} . Considering the thermal system has infinite dimensions, the N4SID models



(a) Electro-mechanical subsystem



(b) Thermo-mechanical subsystem

Fig. 8. Normal case identification results

with low order cannot approximate T_{ex} satisfactorily (see Fig. 8(b)). It can also be found that although the high order model leads to improved accuracy, T_{ex} still cannot be properly predicted. When the proposed PSO assisted RBF network is used, T_{ex} can be estimated accurately, as shown in Fig. 8(b), which demonstrates the effectiveness of the proposed method in the thermo-mechanical subsystem modeling.

To quantify the accuracy of different models, two indices are used to illustrate both the absolute error and the relative error. The first index is the MSE defined in (9). The second index is the Mean Absolute Percentage Error (MAPE), which is defined as [29]

$$MAPE = \frac{100\%}{n} \sum_{i=1}^n \frac{f(i) - a(i)}{a(i)} \quad (10)$$

where $f(i)$ and $a(i)$ denote the forecast and actual values for the i th data. n is the length of the recorded data.

The MSE and MAPE of the model outputs are presented in Table I to illustrate both the absolute error and the relative error. As presented in Table I, both the MSE and MAPE decrease significantly when a large system order is selected for the state space model, which is consistent with previous discussions. However, higher order models imply greater computational costs, and are thus not suitable for modeling when

there is a requirement for the calculation speed. The PSO-assisted RBF model can provide better results than the N4SID on both electro-mechanical and thermo-mechanical subsystems. But it should be noticed that the accuracy difference between the N4SID and the RBF network on the electro-mechanical subsystem identification, is not as obvious as the thermo-mechanical subsystem. The N4SID model is of similar accuracy to the RBF network in modeling the electro-mechanical subsystem, and it provides the internal state estimation as mentioned above. Therefore, the dominant model and the AIC model with lower orders, are more suitable for the electro-mechanical subsystem modeling, while the PSO assisted RBF network is better at thermo-mechanical subsystem modeling.

TABLE I
THE MSE OF THE NORMAL CASE IDENTIFICATION TEST

| Model name | Power output | | Exhaust gas temperature | |
|------------------------------|--------------|-------|-------------------------|-------|
| | MSE | MAPE | MSE | MAPE |
| Dominant model (order: 2) | 0.170 | 1.553 | 264.855 | 2.126 |
| AIC based model (order: 7) | 0.157 | 1.317 | 265.229 | 2.136 |
| High order model (order: 80) | 0.115 | 1.119 | 29.530 | 0.631 |
| PSO-Assisted RBF model | 0.073 | 0.730 | 1.459 | 0.090 |

2) *Saturation Consideration:* In this test, another group of data is added for training in order to incorporate the MT state saturation. As highlighted in the previous section, the MT output may saturate in some scenarios due to the low gas pressure or generator speed constraints. To estimate the saturation, state variables obtained from the N4SID are utilized to estimate the MT engine speed. As shown in Fig. 9, the MT speed and power outputs within the range of 5 kW and 20 kW can be approximated accurately. Yet, some mismatches exist between the linear model predicted output and the actual output when the power output is above 20 kW, as shown in the green line and black line of Fig. 9(b). In addition, it can be seen that the output saturation is consistent with the engine speed variation. Therefore, the MT power output under saturation can be captured with the predefined speed constraint according to (8), as illustrated in Fig. 9(a). It can be seen from Fig. 9(b) that although some mismatches exist in the output prediction, the results are generally acceptable and thus useful in practice.

The performance of the thermo-mechanical subsystem model is also checked using the same period of saturation training data. It can be observed from Fig. 9(c) that the exhaust gas temperature is predicted well in the whole training sample data range. Even for the time that saturations and low load levels occur, it can still produce a close enough prediction, which indicates that the obtained model is able to capture the nonlinear characteristics of the MT even beyond a certain amount of the designed operating range.

B. Model Verification

In order to demonstrate the robustness of the proposed modeling method, another case with low load operating scenarios is investigated. Both the increase and decrease of the power output are studied. As shown in Fig. 10, the model outputs are close to the measured results in most scenarios. It can also be observed that the two subsystem models have different capabilities in handling the low load conditions, due to linear

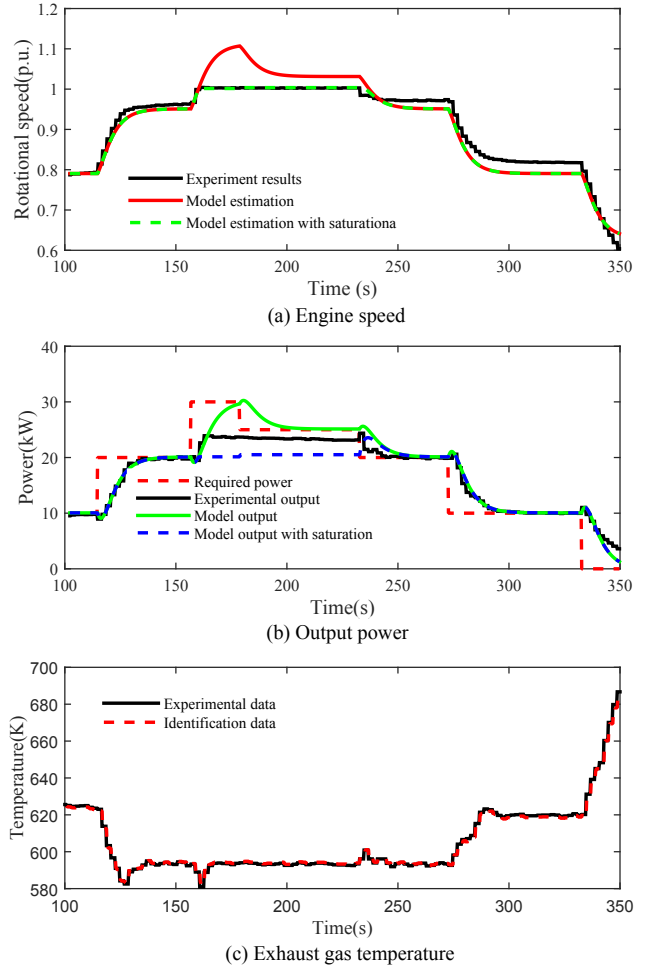


Fig. 9. Saturation case identification results.

and nonlinear characteristics of the two models in essence. On one hand, the electro-mechanical subsystem model output deviates from the experiment data when the power output is lower than 5 kW (see the right area of the dashed brown line). The outputs of the model with and without saturations are close to each other, since no saturations occurred in this case. On the other hand, the thermo-mechanical subsystem model can still obtain a good result although a minor mismatch can be found in the low load area.

Note that the proposed model can not only predict the behaviors of the MT heat and electric outputs in normal states, but also take into account the saturation status. Thus, it allows the simulation of long-term operation of MTs in smart applications with low computational complexity, which can be used to analyze the relationship between the smart grid and other energy systems. By quantifying the inter-relations between the thermal system and the heat system in both normal and saturation states, the proposed model could assist coordinating the thermal and electrical systems of the microgrid. For example, when a MT is used to smooth the fluctuated renewable generation output, the relative heat output can be estimated, which can then be used in the heat system management. The proposed model can also help avoid

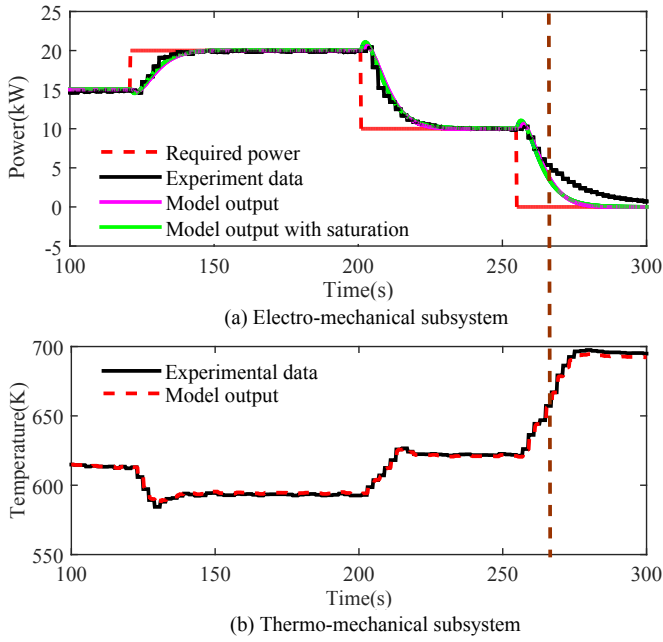


Fig. 10. Comparison of experiment data and model outputs.

scheduling failures of the smart grid caused by natural gas network constraints during the MT output adjustment process.

It is worth mentioning that characteristics of MTs are not the same when the external environment changes. Thus, further mechanism analysis and more training data, such as inlet pressure, exhaust gas flow volume, etc. are required to ensure the model accuracy in practice. Better results may be obtained if these can be incorporated into the modeling process. In future work, MTs from other manufacturers will be utilized as well to further test the performance of the proposed method. Additionally, since the PSO is employed to facilitate the RBF model construction, the computational time is inevitably significantly increased and not ensured due to the stochastic nature of the algorithm. Thus, the proposed method is recommended only when the running time is not important. For online applications, other deterministic initialization schemes can be utilized.

VI. CONCLUSION

In this paper, an integrated modeling method is proposed for MT heat and electric output predictions in different operating modes. To achieve this, the feasibility to decouple thermo-mechanical and electro-mechanical processes is firstly analyzed. Then a three-stage subspace identification method is presented to model the electro-mechanical subsystem output characteristics and key states of a MT, incorporating the operating saturation estimation. Further, a PSO assisted RBF model is employed to describe the thermo-mechanical subsystem behavior. Experimental results confirm the effectiveness and accuracy of the obtained models in a variety of scenarios using a Capstone C30 MT installed in a microgrid testbed.

The results demonstrate that the obtained electro-mechanical subsystem model at lower orders can predict the power output well, which agrees with previously reported theoretical and

experimental findings. Also, the saturation caused by natural gas network pressure constraints can be captured by the obtained model. Additionally, the proposed thermo-mechanical system model can represent the actual thermal dynamic process with good accuracy over a wide operating range. Based on the developed model, an integrated energy management system for microgrids is currently under investigation. This will facilitate the study of the energy system integration in the smart grid. Although the modeling method developed in this paper is designed for microturbines, it can also be used to analyze the interactions and interdependencies between energy infrastructures with different types of coupling units.

APPENDIX

NUMERICAL ALGORITHM FOR SUBSPACE STATE SPACE SYSTEM IDENTIFICATION

The N4SID is implemented through the following steps:

Step 1: Construct the Hankel matrices using U_p and U_f as the past and future inputs matrix, Y_p and Y_f as the past and future outputs matrix and define $W_p \triangleq [U_p \ Y_p]^T \in \mathbb{R}^{(1+l)i \times j}$

Step 2: Left and right multiply Y_f/U_f^\perp with N4SID matrices W_1 and W_2 such that

$$O = W_1(Y_f/U_f^\perp)W_2 = I(Y_f/U_f^\perp)(W_p/U_f^\perp)^\dagger W_p \quad (11)$$

where \dagger represents Moore-Penrose pseudoinverse, U_f^\perp is the complimentary space of U_f , and I stands for space subtraction.

Step 3: Perform singular value decomposition on (12). Use the number of relative large singular values or specified order as system order estimation.

$$O = [U_1 \ U_2] \begin{bmatrix} S_1 & 0 \\ 0 & S_2 \end{bmatrix} \begin{bmatrix} V_1^T \\ V_2^T \end{bmatrix} \quad (12)$$

Step 4: Obtain the extended observability matrix and estimated state matrix X_i :

$$\hat{\Gamma} = W_1^{-1}U_1S_1^{1/2}, \quad X_i = S_1^{1/2}V_1^T W_2^{-1} \quad (13)$$

Step 5: Estimate the system matrix based on the extended observability matrix:

$$A = (\hat{\Gamma})^\dagger \bar{\Gamma}, \quad C = \hat{\Gamma}(1:l,:) \quad (14)$$

where l is the number of outputs; $\hat{\Gamma}$ represent $\hat{\Gamma}$ without the last l rows; $\bar{\Gamma}$ represents $\hat{\Gamma}$ without the first l rows.

Step 6: Calculate matrices B and D by solving the following over-determined equations in a least-square sense:

$$\begin{bmatrix} \hat{X}_{i+1} \\ U_i \end{bmatrix} = \begin{bmatrix} S_1 & 0 \\ 0 & S_2 \end{bmatrix} \begin{bmatrix} \hat{X}_i \\ U_i \end{bmatrix} + \epsilon \quad (15)$$

where ϵ represents the residual matrix. \hat{X}_i and \hat{X}_{i+1} are the estimated state sequences.

ACKNOWLEDGMENT

The authors would like to thank Mr David McIntyre of Queen's University Belfast, for proofreading our manuscripts. The authors would also like to thank the handling editor and the reviewers for their constructive comments.

REFERENCES

- [1] H. Lund, A. N. Andersen, P. A. Østergaard, B. V. Mathiesen, and D. Connolly, "From electricity smart grids to smart energy systems—a market operation based approach and understanding," *Energy*, vol. 42, no. 1, pp. 96–102, 2012.
- [2] X. Zhang, G. G. Karady, and S. T. Ariaratnam, "Optimal allocation of CHP-based distributed generation on urban energy distribution networks," *Sustainable Energy, IEEE Transactions on*, vol. 5, no. 1, pp. 246–253, 2014.
- [3] A. Saha, S. Chowdhury, S. Chowdhury, and P. Crossley, "Modeling and performance analysis of a microturbine as a distributed energy resource," *Energy Conversion, IEEE Transactions on*, vol. 24, no. 2, pp. 529–538, 2009.
- [4] S. Massucco, A. Pitto, and F. Silvestro, "A gas turbine model for studies on distributed generation penetration into distribution networks," *Power Systems, IEEE Transactions on*, vol. 26, no. 3, pp. 992–999, 2011.
- [5] H. Nern, H. Kreshman, F. Fischer, and H. Eldin, "Modeling of the long term dynamic performance of a gas turbo generator set," in *Control Applications, 1994., Proceedings of the Third IEEE Conference on*. IEEE, 1994, pp. 491–496.
- [6] H. Nikkhajoei and M. R. Iravani, "A matrix converter based micro-turbine distributed generation system," *Power Delivery, IEEE Transactions on*, vol. 20, no. 3, pp. 2182–2192, 2005.
- [7] S. Grillo, S. Massucco, A. Morini, A. Pitto, and F. Silvestro, "Microturbine control modeling to investigate the effects of distributed generation in electric energy networks," *Systems Journal, IEEE*, vol. 4, no. 3, pp. 303–312, 2010.
- [8] X. Xu, H. Jia, H.-D. Chiang, D. Yu, and D. Wang, "Dynamic modeling and interaction of hybrid natural gas and electricity supply system in microgrid," *Power Systems, IEEE Transactions on*, vol. 30, no. 3, pp. 1212–1221, 2015.
- [9] K. Li, S. Thompson, and J. Peng, "Modeling and prediction of NOx emission in a coal-fired power generation plant," *Control Engineering Practice*, vol. 12, no. 6, pp. 707–723, 2004.
- [10] X. Hong, S. Chen, Y. Gong, and C. J. Harris, "Nonlinear equalization of hammerstein OFDM systems," *Signal Processing, IEEE Transactions on*, vol. 62, no. 21, pp. 5629–5639, 2014.
- [11] C. Abeykoon, P. J. Martin, K. Li, and A. L. Kelly, "Dynamic modeling of die melt temperature profile in polymer extrusion: Effects of process settings, screw geometry and material," *Applied Mathematical Modeling*, vol. 38, no. 4, pp. 1224–1236, 2014.
- [12] A. E. Ruano, P. J. Fleming, C. Teixeira, K. Rodríguez-Vázquez, and C. M. Fonseca, "Nonlinear identification of aircraft gas-turbine dynamics," *Neurocomputing*, vol. 55, no. 3, pp. 551–579, 2003.
- [13] H. Asgari, M. Venturini, X. Chen, and R. Sainudin, "Modeling and simulation of the transient behavior of an industrial power plant gas turbine," *Journal of Engineering for Gas Turbines and Power*, vol. 136, no. 6, p. 061601, 2014.
- [14] R. Bettocchi, M. Pinelli, P. Spina, and M. Venturini, "Artificial intelligence for the diagnostics of gas turbines-Part I: Neural network approach," *Journal of engineering for gas turbines and power*, vol. 129, no. 3, pp. 711–719, 2007.
- [15] H. Nikpey, M. Assadi, and P. Breuhaus, "Development of an optimized artificial neural network model for combined heat and power micro gas turbines," *Applied Energy*, vol. 108, pp. 137–148, 2013.
- [16] E. Mohammadi and M. Montazeri-Gh, "A new approach to the gray-box identification of wiener models with the application of gas turbine engine modeling," *Journal of Engineering for Gas Turbines and Power*, vol. 137, no. 7, p. 071202, 2015.
- [17] Z. Li, D.-H. Wang, Y.-L. Xue, and D.-H. Li, "Research on ways of modeling of micro gas turbines (ii): Reduction and analysis," *Power Engineering*, vol. 2, p. 002, 2005.
- [18] X. Wang and H.-D. Chiang, "Analytical studies of quasi steady-state model in power system long-term stability analysis," *Circuits and Systems I: Regular Papers, IEEE Transactions on*, vol. 61, no. 3, pp. 943–956, 2014.
- [19] Y. Ruan, Q. Liu, W. Zhou, R. Firestone, W. Gao, and T. Watanabe, "Optimal option of distributed generation technologies for various commercial buildings," *Applied Energy*, vol. 86, no. 9, pp. 1641–1653, 2009.
- [20] L. Ljung, "System identification: Theory for the user," *PTR Prentice Hall Information and System Sciences Series*, vol. 198, 1987.
- [21] V. Tikhomirov, "On the representation of continuous functions of several variables as superpositions of continuous functions of one variable and addition," in *Selected Works of AN Kolmogorov*. Springer, 1991, pp. 383–387.
- [22] J.-X. Peng, K. Li, and G. W. Irwin, "A novel continuous forward algorithm for RBF neural modeling," *Automatic Control, IEEE Transactions on*, vol. 52, no. 1, pp. 117–122, 2007.
- [23] J. Deng, K. Li, G. W. Irwin, and M. Fei, "Two-stage RBF network construction based on particle swarm optimization," *Transactions of the Institute of Measurement and Control*, vol. 35, no. 1, pp. 25–33, 2013.
- [24] K. Li, J.-X. Peng, and G. W. Irwin, "A fast nonlinear model identification method," *Automatic Control, IEEE Transactions on*, vol. 50, no. 8, pp. 1211–1216, 2005.
- [25] C. Wang, X. Yang, Z. Wu, Y. Che, L. Guo, S. Zhang, and Y. Liu, "A highly integrated and reconfigurable microgrid testbed with hybrid distributed energy sources," *IEEE Transactions on Smart Grid*, vol. 7, no. 1, pp. 451–459, 2016.
- [26] J. Devlin, K. Li, P. Higgins, and A. Foley, "The importance of gas infrastructure in power systems with high wind power penetrations," *Applied Energy*, vol. 167, pp. 294–304, 2016.
- [27] *C30 MicroTurbine Natural Gas*, Capstone Turbine Corporation, <http://www.capstoneturbine.com/products/c30>.
- [28] D. Yue and K. Li, "A modeling approach of DC link of micro-gas turbine generation system," *POWER SYSTEM TECHNOLOGY-BEIJING*, vol. 32, no. 3, p. 13, 2008.
- [29] Y.-S. Lee and L.-I. Tong, "Forecasting nonlinear time series of energy consumption using a hybrid dynamic model," *Applied Energy*, vol. 94, pp. 251–256, 2012.



Xiandong Xu (M'15) received his B.Sc. and Ph.D. degrees in Electrical Engineering from Tianjin University, Tianjin, China, in 2009 and 2015 respectively.

He is currently working as a Research Fellow at Queen's University Belfast, UK. His research focuses on energy infrastructure modeling, optimization, and reliability analysis.



Kang Li (M'05-SM'11) received the B.Sc. degree in industrial automation from Xiangtan University, Xiangtan, China, in 1989, the M.Sc. degree in control theory and applications from Harbin Institute of Technology, Harbin, China, in 1992, the Ph.D. degree in control theory and applications from Shanghai Jiaotong University, Shanghai, China, in 1995, and the D.Sc. degree in science from Queens University Belfast, Belfast, U.K., in 2015.

He is currently a Professor in Intelligent Systems and Control with the School of Electronics, Electrical Engineering, and Computer Science, Queens University Belfast. His research interests include nonlinear system modeling, identification and control, and bioinspired computational intelligence, with applications to energy and power systems, renewable energies, smart grid, electric vehicles, polymer processing, the development of advanced control technologies for decarbonizing the entire energy systems from top to tail, and the development of a new generation of low-cost minimally invasive monitoring system and intelligent control platforms for energy-intensive industries.



Hongjie Jia (M'04) received his B.S., M.S., and Ph.D. degrees in electrical engineering from Tianjin University, China, in 1996, 1998, and 2001 respectively.

He is a Professor of Tianjin University. His research interests include power system stability analysis and control, distribution network planning, renewable energy integration, and smart grids.



Xiaodan Yu received her B.S., M.S., and Ph.D. degrees in the electrical engineering from Tianjin University, China, in 1996, 1998, and 2013 respectively.

She is currently an Associate Professor at Tianjin University. Her research interests include power system stability, integrated energy system, electric circuit theory and smart grids.



Jing Deng received his Ph.D. degree in electrical engineering from Queens University Belfast, Belfast, U.K., in 2011.

He then started to work as a Research Fellow with Queens University Belfast. His research interests include nonlinear system modeling, optimization, and fuzzy control with their applications to smart grid, electric vehicles, and renewable energies.



Yunfei Mu (M'11) was born in Hebei, China. He received his PhD degree in the School of Electrical Engineering and Automation, Tianjin University, Tianjin, China, in 2012.

He is now an Associate Professor of Tianjin University. His main research interests include power system security analysis, electric vehicles and smart grids.